ELSEVIER

Journal of Wind Engineering
and Industrial Aerodynamics 87 (2000) 187–201

JOURNAL OF wind engineering AND industrial aerodynamics

www.elsevier.com/locate/jweia

# Study on the short-term characteristics of the wind field in Keelung, Taiwan

John Z. Yim*, Chun-Ren Chou

*Department of Harbour and River Engineering, National Taiwan Ocean University, 2, Bee-Ning Road, 20224 Keelung, Taiwan, People's Republic of China*

Accepted 3 July 2000

**Abstract**

Short-term characteristics of the wind field and temperature measured in Keelung, Taiwan were studied. The fluctuating components of measured wind speeds and the temperature were fitted with statistical models found in the literature. In general, the distributions of the fluctuating components are skewed, having more pronounced peaks as compared with the symmetric Gaussian model. The Edgeworth's type A Gram–Charlier series expansion was found to be more adequate in describing the statistical properties of the winds. Spectra of the turbulent wind fluctuations are found to follow the $-\frac{5}{3}$-power law at the high-frequency tail. The spectra of the temperature, on the other hand, are usually flat in this region, resembling that of the white noise. 

*Keywords:* Gaussian distribution; Gram–Charlier series; Turbulent fluctuations

## 1. Introduction

Knowledge of the regional wind fields is important for a variety of reasons. Civil engineers may need to estimate the extreme wind speeds in designing of structures [1]. To study and model the spread of pollutants, environmental scientists need to know the standard deviations of the fluctuation velocity components [2]. The auto- and cross-spectral characteristics of a turbulent wind field can provide vital information for the simulation of the wind fields [3]. Furthermore, wind stresses are the dominant factor in generating waves on the ocean surface. The waves thus

*Corresponding author. Tel./fax: +886-2-2463-3684.
*E-mail address:* b0052@ind.ntou.edu.tw (J.Z. Yim).

0167-6105/00/$ - see front matter 
PII: S0167-6105(00)00036-2

generated, can further interact with the overlaying turbulent wind field, and thereby enhance the momentum and gas exchange between the air–sea interface [4].

Roughly speaking, as a first approximation, any wind velocity–time series can be considered as a linear combination of at least three factors caused by occurrences at different scales. The most important factor is played by the weather system at the time of measurements, which can be called the global effect. It plays the most dominant part in determining the ultimate outcome of the wind velocity. The second factor is the local effect, which reflects the influences on the time series imposed by the geographical conditions of the measuring site. The third factor is the so-called random effect, which is the result of random disturbances inherently imposed by the nature during measurements. Breckling [5] has demonstrated that wind records containing speeds and directions can be divided into four components: the prevailing wind, a land- and sea-breeze cycle, a storm component and a residual component of random fluctuations. Since our records are relatively short, in the present paper, we concentrate on the characteristics of short-term fluctuations contained in wind records.

Quite often, wind records provided by meteorological bureaus are in the form of averaged 10 min wind speeds and directions. Records in this form may be appropriate for studies of long-term statistics, and predictions of extreme winds are not suitable for short-term statistical analysis. One needs continuous recordings with relatively high sampling rate to study the short-term characteristics of a wind field. The Department of Harbour and River Engineering of the National Taiwan Ocean University has recently acquired a subvention from the Ministry of Education, ROC, for the study of air–sea interaction. An ultrasonic anemometer was installed therewith. While the experiments are still ongoing, the present article presents some preliminary results.

In the following, we further divide this article into four parts. Section 2 contains a short description of the measuring site and the instrumentation. In Section 3, we describe shortly the methods applied for data processing, as well as the models we used. In Section 4, we present results of our analyses together with discussions. It will be shown that the three turbulent velocity components can be better modelled by the Gram–Charlier series expansion, while the fluctuating component of the temperature are better described by the Gaussian model. With a short conclusion in Section 5 we close this paper.

## 2. The measuring site and the instrumentation

### *2.1. The measuring site*

The Keelung city is located in the northeastern part of Taiwan. Mountains surround three sides of the city, while the other side is open to the Pacific Ocean. While relatively strong winds often occur in winter seasons with the prevailing direction of NE or NNE, relatively mild winds are predominant in the summer seasons. The dominant wind direction in summer seasons is SW. Typhoon invasions

will occasionally occur in summer seasons. Measured wind speeds during the passage of typhoons can be very high. According to the records of the Central Weather Bureau (CWB) of ROC, for the period 1984–1994, approximately 3.4% of the recorded wind speeds have values in the range from 13.9 to 17.1 m/s. All the high winds were measured in winter seasons. It should be mentioned, however, that this statistics are for the so-called well-behaved weather conditions, where the extreme winds from typhoon are excluded. The measuring station is located atop the roof of the Department of the Harbour and River Engineering of the National Taiwan Ocean University. The building is located close to the coast. Fig. 1 shows a schematic sketch of the geographical location of the measuring site.

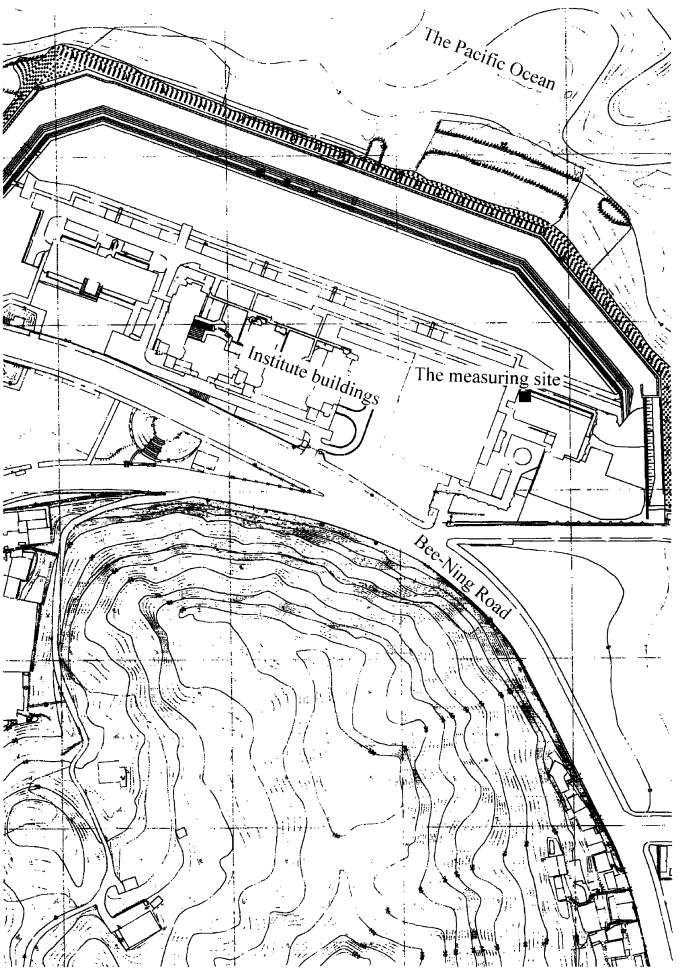


Fig. 1. Geographical location of the Keelung city.

### 2.2. The instrumentation

A 3D ultrasonic anemometer of type TJ-61B from KAIJO Corporation was mounted on a mast. The mast is anchored on the roof of the building of the Department. Total height of the anemometer is 26 m above sea level. According to the factory specifications, with a resolution of 0.005 m/s, the anemometer is capable of measuring winds up to 60 m/s. Temperature fluctuations can be measured from $-10^{\circ}$C to $40^{\circ}$C, with a resolution of $0.025^{\circ}$C. A more detailed description concerning the principle of the anemometer can be found in Ref. [6].

The positive $x$-axis of the anemometer is oriented toward the west, while the positive $y$-axis is toward the south. Variations of wind speeds, as well as the temperature, were recorded continuously with a sampling rate of 20 Hz. Data recording was carried out continuously till the present day ever since it started on 20 May 1998. The recorded data are then stored in files separated by the hours of the day. An hourly data thus contains approximately 72 000 data points. No corrections of the true wind directions were made during the calculation at this moment. All analyses were conducted on an IBM-compatible personal computer with a Pentium III processor.

## 3. Analyses of the data

Due to occasional unsteadiness of the electrical power supply, the recorded data may sometimes contain erroneous spikes, or outliers. A program was therefore written to "smooth" the raw data. After that the possible outliers have been detected and smoothed, the data were zero-meaned and detrended in the usual manner [7].

For the statistical calculations, the data were first normalized: $\hat{x}_i = x_i'/x_{\mathrm{rms}}'$, where $x' = (u', v', w', \theta')$, and $x_{\mathrm{rms}}'$ represents the root-mean-square value of the respective variable. Afterwards, the data were sorted in ascending order. For simplicity, we will drop the hatch above the variable $x$ in the following. To study the possible distributions of the turbulent fluctuations of measured data, we have used two statistical models. The first one is the well-known Gaussian distribution, which can be expressed as

$$p(x,\mu,\sigma) = \frac{1}{\sigma\sqrt{2\pi}} \exp\left[-\frac{(x-\mu)^2}{2\sigma^2}\right], \tag{1}$$

where $x$ denotes the normalized fluctuating components, $\mu$ is the mean value, and $\sigma$ is the standard deviation. The second model is the Edgeworth's type A Gram–Charlier series expansion written here as

$$p(x) = \frac{1}{\sqrt{2\pi K_2}} \exp\left[-\frac{t^2}{2}\right]\left[1 + \frac{1}{6}K_3H_3 + \frac{1}{24}K_4H_4 + \frac{K_5H_5}{120} + \frac{(H_6 + 10H_3^2)}{720}H_6 + \cdots\right], \tag{2}$$

where as before, $x$ is the dimensionless fluctuations, and $\lambda_n$ the $n$th cumulant, which in terms of the $n$th central moments, $\mu_n$, can be expressed as [8]

$$\lambda_1 = \mu_1 = 0, \tag{3a}$$

$$\lambda_3 = \mu_3, \tag{3b}$$

$$\lambda_4 = \mu_4 - 3\mu_2^2, \tag{3c}$$

$$\lambda_5 = \mu_5 - 10\mu_3\mu_2, \tag{3d}$$

$$\lambda_6 = \mu_6 - 15\mu_4\mu_2 - 10\mu_3^2 + 30\mu_2^3, \tag{3e}$$

where the $n$th central moment is defined as

$$\mu_n = E[(x-\mu)^n]. \tag{4}$$

Furthermore,

$$t = \frac{x}{\sigma}, \tag{5}$$

$$K_n = \frac{\lambda_n}{\sqrt{\lambda_2^n}}. \tag{6}$$

$H_n$ is the $n$th Hermite polynomial with

$$H_3(t) = t^3 - 3t, \tag{7a}$$

$$H_4(t) = t^4 - 6t^2 + 3, \tag{7b}$$

$$H_5(t) = t^5 - 10t^3 + 15t, \tag{7c}$$

$$H_6(t) = t^6 - 15t^4 + 45t^2 - 15. \tag{7d}$$

Eq. (2) can be derived either from orthogonal polynomials, or from the cumulant generating function [8]. Longuet-Higgins [9] has derived it from the latter. He showed that, as the nonlinearity of the water waves becomes no more negligible, the probability distribution of the water surface fluctuations will deviate from normality, and it is then more appropriate to use this model. This is especially true for wind-wave flume experiments with active wind wave generation, which was called as "strongly nonlinear process" by Toba [10], as was demonstrated by Huang and Long [11]. However, when the Gram–Charlier series is applied, it has one main drawback. This model can occasionally have negative values, which makes it unrealistic as a model for probability function. Fortunately, our experiences have shown that, except for temperature fluctuations, this does not occur very often for well-behaved weather conditions.

All the statistical fits were checked with goodness-of-fit test. At first, the $\chi^2$-test was carried out. As is well known, an estimate of the degree of freedom is needed when the $\chi^2$ goodness-of-fit test is to be carried out. Since the authors are unaware of methods for the estimation of the degrees of freedom for the Gram–Charlier series, the two statistical models were further verified using the Kolmogorov–Smirnov goodness-of-fit test.

Another way to evaluate the possible distribution of the sample without assessing the merit or demerit of any statistical models is through the skewness and kurtosis of the sample set. Defining the $m$th central moments as

$$\mu_m = E(x - \mu_1')^m, \tag{8}$$

where $\mu_1'$ is the mean, and use this equation to estimate the $m$th moment of a sample set:

$$m_m = \frac{\sum_{i=1}^{N} (x_i - \bar{x})^m}{N}, \tag{9}$$

where $\bar{x}$ is the data mean. The skewness and kurtosis are related to, respectively, the third and fourth moments about the mean. They can be estimated through [12]

$$\sqrt{b_1} = \frac{m_3}{\sqrt{m_2^3}}, \tag{10}$$

$$b_2 = \frac{m_4}{m_2^2}. \tag{11}$$

When the underlying distribution is normal or approximately normal, one should have $\sqrt{b_1} \approx 0$ and $b_2 \approx 3$.

Auto- and cross-spectra of the four fluctuating components were also calculated. In order to increase the degrees of freedom (DOF) in the spectral estimates, records were separated into several nonoverlapping segments. Each segment has 1024 data points. A partial cosine taper function was added to every segment to minimize side lobe leakage. The data were then fast fourier transformed (FFT) to obtain a rough two-sided spectral estimate. Ensemble averaging of the rough spectral densities was then performed to obtain a smoothed estimate. The spectral densities were also smoothed in the frequency domain with a Hanning window to increase the DOF of the resulting spectra. All final spectral estimates have 140 DOF, with a frequency resolution of $\Delta f \approx 0.019$ Hz.

In the present article, we present results of two months, i.e., June and December, representing, respectively, the weak southwestern winds in the summer, and the relatively strong northeastern winds in the winter. According to our data, approximately 95.56% of the measured winds in June have speeds less than 3.0 m/s. As a comparison, approximately 50% of the measured wind speeds in December are larger than 3.0 m/s. As an example of extrema, we present records measured on June 8 at 17 : 00–17 : 59 p.m., and on December 10 at 17 : 00 –17 : 59 a.m., both were from the year 1998. The mean wind speeds for these two time dates are, respectively, 2.05 and 7.20 m/s, whereas the maximum wind speeds (gust) are 9.56 and 14.60 m/s.

## 4. Results and discussion

### 4.1. The cases with weak winds

Fig. 2 shows the distribution of the normalized longitudinal velocity fluctuations, $u'/u'_{\text{mean}}$, fitted with the two models applied in this paper. The data were measured on

June 8 from 17:00 to 17:59 p.m. As mentioned earlier, the mean wind speed is 2.05 m/s. It can be seen from Fig. 2 that the histogram shows a marked peak at $u'/u'_{\mathrm{rms}} = 0$, which is typical for all the data studied here. It can also be seen that the Gram–Charlier series expansion can fit the peak of the histogram better than the Gaussian. The parameters estimated from the third and the fourth moments of the sample set, i.e., the skewness and kurtosis are, respectively, $\sqrt{b_1} \approx 0.04$, $b_2 \approx 3.95$. This also indicates that the underlying distribution is almost symmetric, but with a pronounced peak, as compared with the normal distribution.

The probability distributions of the normalized lateral and the vertical velocity fluctuations from the same data set as in Fig. 2 are shown, respectively, in Figs. 3 and 4. As can be seen from these figures, the results are similar to that shown in Fig. 2, except that the distribution for the lateral components in Fig. 3, are skewed to the left. The parameters for the skewness and kurtosis for the two fluctuating velocity components are, respectively, $\sqrt{b_1} \approx -0.61$, $b_2 \approx 4.16$ for the $v'/v'_{\mathrm{rms}}$ component; and $\sqrt{b_1} \approx 0.003$, $b_2 \approx 3.55$ for the $w'/w'_{\mathrm{rms}}$ component.

From Figs. 2–4, it is seen that the dimensionless turbulent velocity fluctuations all have pronounced peaks near the origin as compared with the Gaussian distribution. It should be mentioned that the results presented here are quite general; almost all of the cases analyzed by us have similar trends. Table 1 summarizes the averaged values of these two parameters for the months June and December. It can be seen from Table 1 that the mean values of the kurtosis are always larger than 3. This indicates

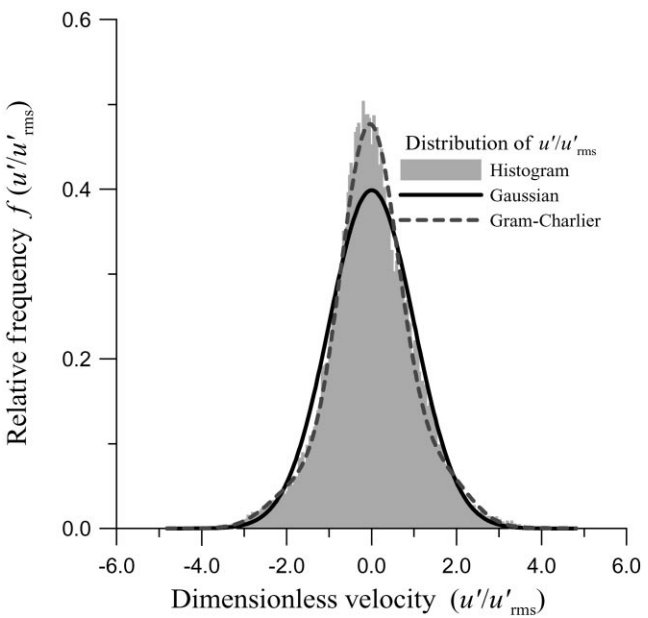


Fig. 2. Distributions of longitudinal velocity components fitted with the Gaussian (unbroken line) and the Gram–Charlier series expansions (broken line). Data recorded on 8 June 1998 from 5:00 to 5:59 p.m.

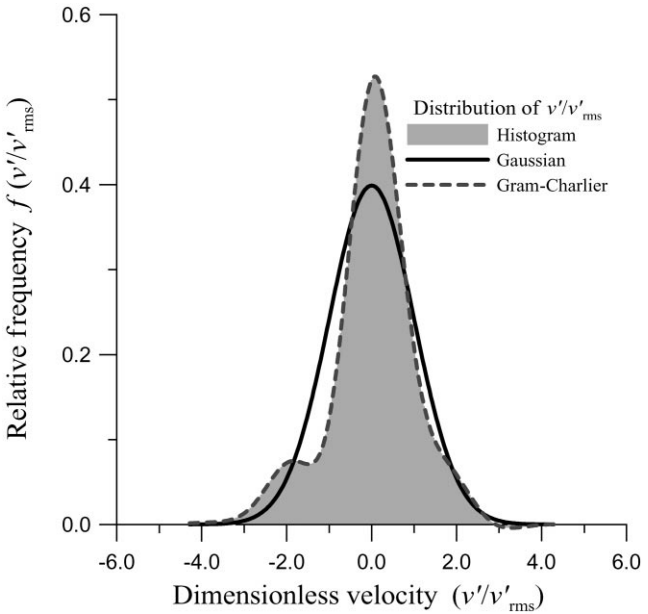


Fig. 3. Distributions of lateral velocity components fitted with the Gaussian (unbroken line) and the Gram–Charlier series expansions (broken line). Data recorded on 8 June 1998 from 5:00 to 5:59 p.m.

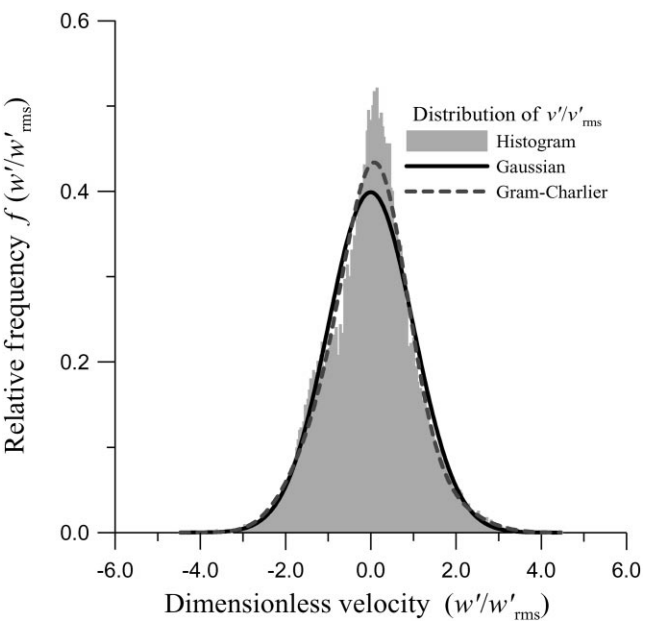


Fig. 4. Distributions of vertical velocity components fitted with the Gaussian (unbroken line) and the Gram–Charlier series expansions (broken line). Data recorded on 8 June 1998 from 5:00 to 5:59 p.m.

Table 1
Averaged values of skewness and kurtosis of the velocity components

| Velocity component | Month | June | | December | |
|---|---|---|---|---|---|
| | | Skewness $\sqrt{b_1}$ | Kurtosis $b_2$ | Skewness $\sqrt{b_1}$ | Kurtosis $b_2$ |
| $u'$ | Minimum | −2.73 | 1.37 | −5.54 | 1.15 |
| | Maximum | 1.84 | 13.21 | 10.55 | 203.46 |
| | Average | 0.02 | 3.98 | 0.03 | 4.96 |
| $v'$ | Minimum | −1.92 | 1.53 | −5.27 | 1.34 |
| | Maximum | 1.60 | 8.56 | 4.62 | 67.23 |
| | Average | −0.05 | 3.45 | −0.11 | 3.97 |
| $w'$ | Minimum | −2.05 | 1.22 | −9.40 | 1.16 |
| | Maximum | 2.20 | 26.47 | 5.52 | 121.77 |
| | Average | −0.01 | 5.19 | −0.22 | 5.26 |

that most of the time the probability distributions of the fluctuating velocity components have pronounced peaks. It is also interesting to note that the values of the kurtosis for the month December are always larger than that for the month June. This seems to indicate that the stronger the wind, the more pronounced will be the probability distributions of the velocity components around its mean value. Further studies are needed to ascertain this conjecture.

### 4.2. The results with strong winds

Figs. 5–7 show the results of fitting the two statistical models for the wind speeds measured on December 10, 1998. Notice that in Figs. 5 and 6 both the horizontal velocity components are skewed to the left, and how the curves of the Gram–Charlier series follow the trends. It is also interesting to note that in both figures, the curves of the Gram–Charlier series have negative values at approximately $u'/u'_{\mathrm{rms}}$ or $v'/v'_{\mathrm{rms}}$, $\approx$2.5. This is the main disadvantage of this series expansions mentioned earlier, which makes the series to appear unrealistic for a probability model. Fig. 7 shows that the vertical velocity components are also skewed.

We have also used the two models to study the distributions of the temperature fluctuations. It was found that, in general, only the Gaussian distribution can be used to approximate the distribution of the temperature. The curves of the Gram–Charlier series often undulate strongly with unrealistic positive and negative values around the axis of $f(\theta'/\theta'_{\mathrm{mean}}) = 0$. Fig. 8 shows one of the results. The data used in this figure were measured on December 10, 1998 from 5:00 to 5:59 p.m. Only the curve of the Gaussian model is shown. The reason for the misfit of the Gram–Charlier model is not clear at the moment. It seems that the strong fluctuations of the curve is due to the values of the Hermite polynomial. But how these were affected by the data must wait for further studies.

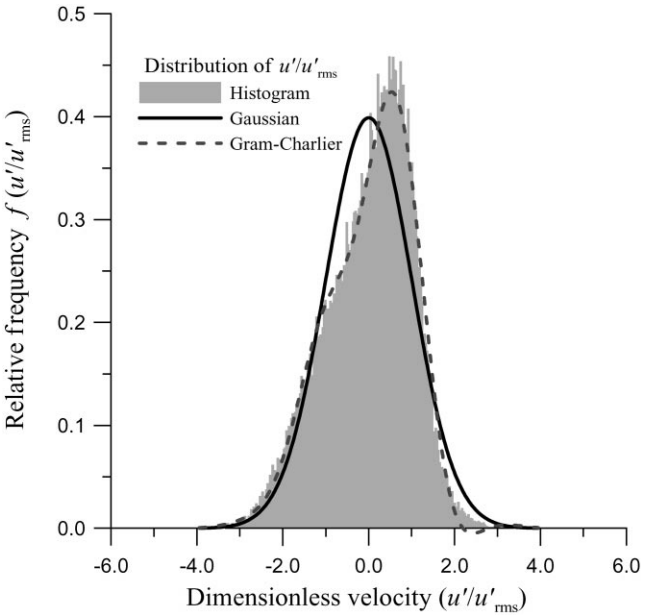


Fig. 5. Distributions of longitudinal velocity components fitted with the Gaussian (unbroken line) and the Gram–Charlier series expansions (dashed line). Data recorded on 10 December 1998 from 5:00 to 5:59 p.m.

### 4.3. The spectrum of the turbulent fluctuations

Power spectra of the turbulent fluctuating components were also calculated. Fig. 9 shows the spectra of the longitudinal velocity components measured at different daytimes. The abscissa and coordinate were both nondimensionalized using, respectively, the relations

$$\hat{f} = \frac{fz}{\overline{U}}, \tag{12}$$

$$\hat{S}_{xx}(\hat{f}) = \frac{S_{xx}(f)f}{\sigma_x^2}, \tag{13}$$

where, as before, the variable $x$ denotes fluctuating quantities, $x = (u', v', w', \theta')$, $z$ is the measuring height, $\overline{U}$ is the mean wind speed and $\sigma_x^2$ is the variance of the respective variable.

Also shown in the figure is the theoretical Kolmogorov $-\frac{2}{3}$ line at the high-frequency tail for comparison. The spectra of the other two fluctuating velocity components are similar to Fig. 9, i.e., almost all of them show the typical $-\frac{2}{3}$ slope at the high-frequency tail, and thus will not be presented here. The mean values of the three velocity components, together with that for the temperature, are given in Table 2. From Table 2, it seems safe to conjecture that, for cases with moderate wind

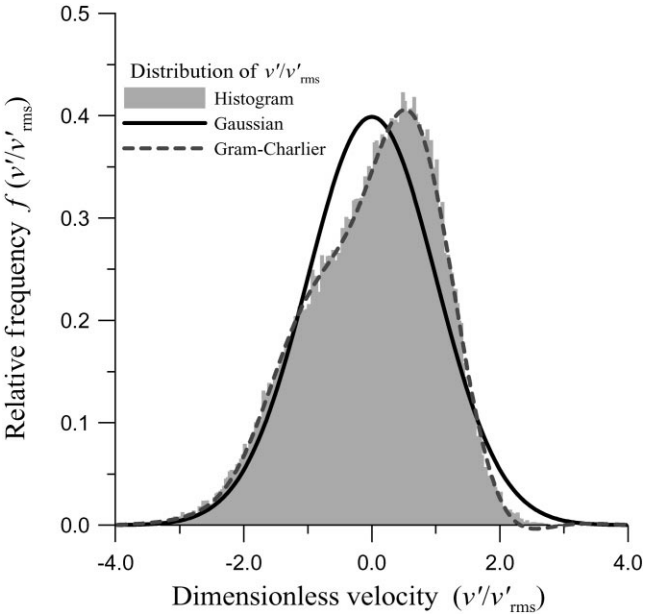


Fig. 6. Distributions of lateral velocity components fitted with the Gaussian (unbroken line) and the Gram–Charlier series expansions (dashed line). Data recorded on 10 December 1998 from 5:00 to 5:59 p.m.

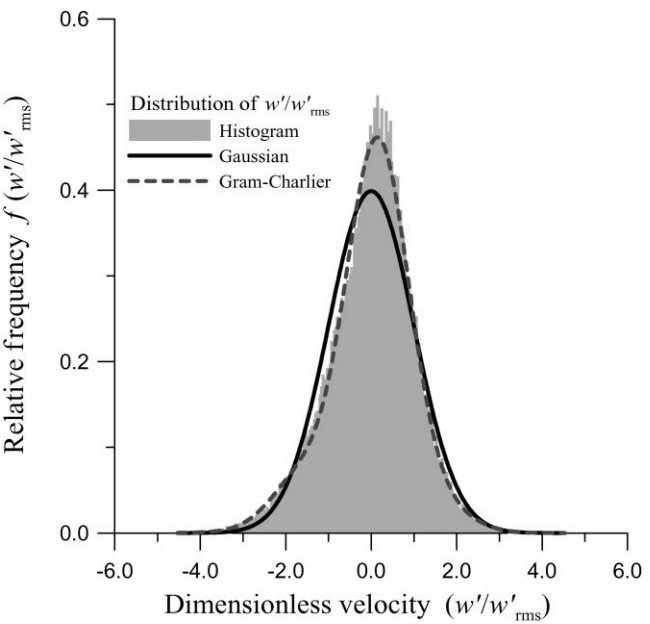


Fig. 7. Distributions of vertical velocity components fitted with the Gaussian (unbroken line) and with the Gram–Charlier series (broken line). Data recorded on 10 December 1998 from 5:00 to 5:59 p.m.

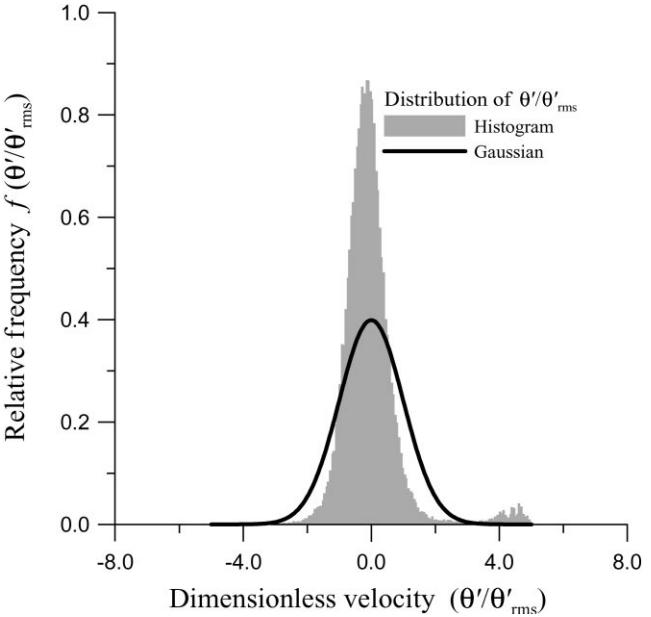


Fig. 8. Distributions of temperature fluctuations fitted with the Gaussian (straight line). Data recorded on 10 December 1998 from 5:00 to 5:59 p.m.

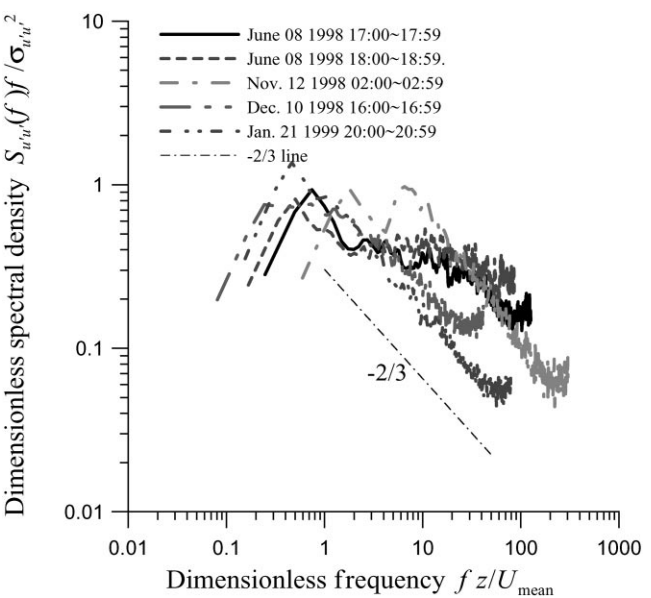


Fig. 9. Normalized spectra of the longitudinal velocity components measured at different daytimes.

Table 2
Average values of the velocity components and temperature for different days of measurement. Format of the date: ddmmyyyy

| Date | Time | $\bar{u}$ (m/s) | $\bar{v}$ (m/s) | $\bar{w}$ (m/s) | $\bar{\theta}$ (°C) |
|---|---|---|---|---|---|
| 08061998 | 5:00–5:59 p.m. | −0.83 | 0.23 | 0.16 | 29.90 |
| 08061998 | 6:00–6:59 p.m. | −0.14 | −0.19 | 0.11 | 29.68 |
| 12111998 | 2:00–2:59 a.m. | 2.79 | −0.78 | 0.20 | 23.63 |
| 10121998 | 4:00–4:59 p.m. | 6.28 | 0.69 | 1.04 | 19.68 |
| 21011999 | 8:00–8:59 p.m. | 3.32 | −1.68 | 0.07 | 19.78 |

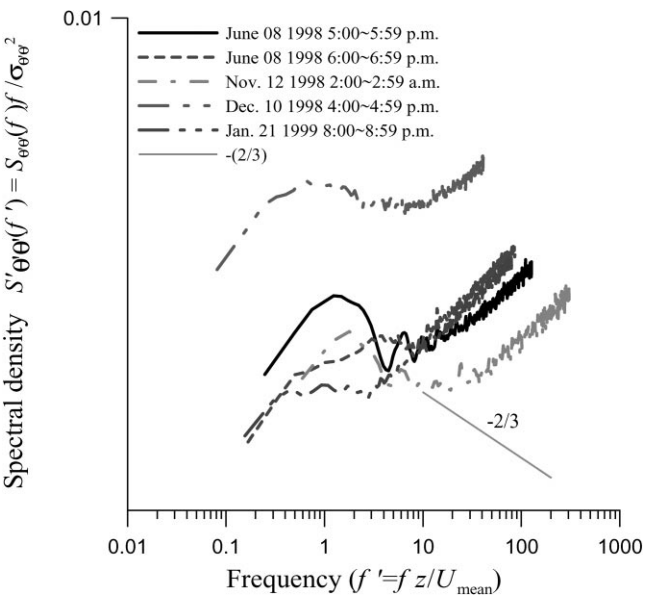


Fig. 10. Normalized spectra of the temperature fluctuations measured at different daytimes.

speeds, all the spectra of the fluctuating velocity components have similar appearances.

However, since at present only one anemometer at a single measuring height is available, the spectra cannot be normalized using the Reynolds stress as was done by many researchers. It is, therefore, impossible at the moment to compare our spectra with the empirical spectra proposed by other researchers [13]. Fig. 10 shows the spectra of the temperature fluctuations. The same data set used for Fig. 9 was used.

The tails of the spectral densities of the temperature fluctuations increase steadily with frequency. These are fictitious and are results due to normalization. In reality, they have flat tails in the high-frequency ranges, which is typical for white noise. To demonstrate this, we have replotted Fig. 10 in dimensional form as Fig. 11. As

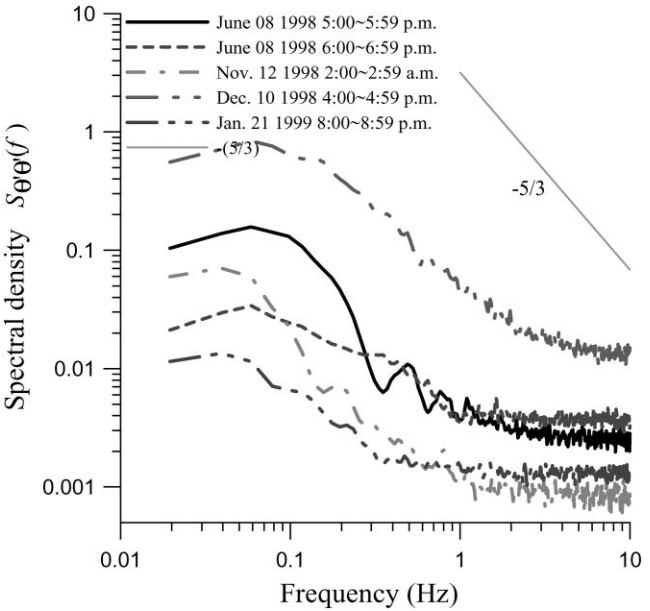


Fig. 11. Spectra of the temperature fluctuations measured at different daytimes.

shown in Table 2, the mean wind speeds associated with the spectra of Figs. 9 and 10 are relatively mild. Maeda and Makino [14] studied the characteristics of the power spectra for strong winds. They found that their power spectra of the lateral wind speed did not agree with the theoretical values, while the opposite is true for longitudinal wind speeds. As our mean wind speeds are relatively mild, no comparison with their results can be made at present.

## 5. Conclusions

Statistical properties of turbulent fluctuations of the three velocity components and temperature have been carried out in this study. For the present, it is concluded that:

- Both the Gaussian distribution and the Gram–Charlier series expansion can be used to model the probability distributions of the fluctuating velocity components of a turbulent wind field. Quite often, the latter model presents better fits when the data are skewed and peaked. However, the Gram–Charlier model may sometimes yield curves that are unrealistic for probability distributions.
- For weak to moderate winds, the spectra of the fluctuating velocity components have forms in the high-frequency range that are in accordance with the theoretical predictions.

- Temperature fluctuations can be approximated with a normal distribution. The Gram–Charlier model often failed to yield reasonable results.
- The high-frequency tails of the spectra for the temperature fluctuations have appearances typical for white noise.

## Acknowledgements

This project is partially supported by the National Science Council, Contract No. NSC-89-2611-E-019-024.

## References

[1] N.J. Cook, The Designer's Guide to Wind Loading of Building Structures, Butterworths, London, 1985.
[2] R.O. Weber, Estimators for the standard deviations of lateral, longitudinal and vertical wind components, Atmos. Environ. 32 (1998) 3639–3646.
[3] J. Mann, Wind field simulation. Prob. Eng. Mech. 13 (1998) 269–282.
[4] S.D. Smith et al., Sea surface wind stress and drag coefficients: the HEXOS results, Boundary-Layer Meteorol. 60 (1992) 109–142.
[5] J. Breckling, The Analysis of Directional Time Series: Applications to Wind Speed and Direction, Springer, Berlin, 1989.
[6] M. Miyake et al., Spectra and cospectra of turbulence over water, Quart. J. R. Met. Soc. 96 (1970) 138–143.
[7] J.S. Bendat, A.G. Piersol, Random data, Analysis and Measurement Procedures, 2nd Edition, Wiley, New York, 1986.
[8] M.K. Ochi, Applied Probability and Stochastic Processes in Engineering and Physical Sciences, Wiley, Singapore, 1992.
[9] M.S. Longuet-Higgins, The effect of non-linearities on statistical distributions in the theory of sea waves, J. Fluid Mech. 17 (1963) 459–480.
[10] Y. Toba, Study on wind waves as a strongly nonlinear phenomenon, in: D.W. Taylor (Ed.), Naval Hydrodynamics, 12th Symposium Office of Naval Research Naval Ship Research and Development Center National Research Council, Naval Study Board, Washington, DC, 1978, pp. 529–540.
[11] N.E. Huang, S.R. Long, An experimental study of the surface elevation probability distribution and statistics of wind generated waves, J. Fluid Mech. 101 (1980) 179–200.
[12] G.J. Hahn, S.S. Shapiro, Statistical Models in Engineering, Wiley, New York, 1967.
[13] S.K. Chakrabarti, Nonlinear Methods in Offshore Engineering, Elsevier, Amsterdam, 1990.
[14] J. Maeda, M. Makino, Power spectra of longitudinal and lateral wind speed near the ground in strong winds, J. Wind Eng. Ind. Aerodyn. 28 (1988) 31–40.